Agricultural and Forest Meteorology 311 (2021) 108701

Contents lists available at ScienceDirect

Agricultural and Forest Meteorology

journal homepage: www.elsevier.com/locate/agrformet

The coupled effect of soil and atmospheric constraints on the vulnerability and water use of two desert riparian ecosystems

Yan Bai [a], Yanlan Liu [b], Lara M. Kueppers [c], Xue Feng [d], Kailiang Yu [e], Xiaofan Yang [f], Xiaoyan Li [f], Jianping Huang [a,*]

[a] College of Atmospheric Sciences, Collaborative Innovation Center for Western Ecological Safety, Lanzhou University, Lanzhou, China
[b] School of Earth Sciences, The Ohio State University, OH, USA
[c] Energy and Resources Group, University of California, Berkeley, CA, USA
[d] Department of Civil, Environmental and Geo-engineering, University of Minnesota, Minneapolis, MN, USA
[e] Princeton Environmental Institute, Princeton University, Princeton, USA
[f] State Key Laboratory of Earth Surface Processes and Resource Ecology, Faculty of Geographical Science, Beijing Normal University, Beijing, China

ARTICLE INFO

Keywords:
Plant hydraulics
Mortality risk
Water use
Evapotranspiration
Water flux
Water stresses

ABSTRACT

Plant response to soil and atmospheric water stresses is the dominant control of Dryland ecosystem functions, affecting water resources, ecosystem stability and biodiversity. The link between water stresses and plant water status is regulated by plant hydraulics, of which the corresponding impact on plant water use and the susceptibility of Dryland ecosystems remains under-explored. We used a plant hydraulic model to describe hydraulic states and water flux of two species (*Populus euphratica* and *Tamarix ramosissima*) in desert riparian ecosystems. We optimized hydraulic parameters and tested the model using observed physiological states and ecosystem water flux. The optimized model was used to evaluate plant hydraulic sensitivity, tree mortality risk, and evapotranspiration under a wide range of water stress scenarios. The model captures the observed leaf water potential, sap-flow and ecosystem evapotranspiration. Our scenario analysis demonstrates that hydraulic sensitivities generally reduce as the water stresses intensify. The results highlight a strong coupled impact of the co-occurrence of soil and atmospheric water stresses on restricting ecosystem water flux and intensifying mortality risk. The assessment of multiple aspects of eco-physiological functions and the stress scenario analysis of desert riparian ecosystems will contribute to a better prediction of ecosystem functions and facilitate resource management under future climate.

1. Introduction

Drylands account for over 45% of the terrestrial land area (Lal, 2004). The dynamics of Dryland ecosystem fluxes, which are primarily driven by soil and atmospheric water stresses, play a dominant role in the trend and variability of the global carbon budget (Ahlström et al., 2015; Biederman et al., 2017; Poulter et al., 2014). Dryland ecosystems are especially susceptible to climate warming and drought (Reed et al., 2012; Schlaepfer et al., 2017). Over the recent decades, drastic changes in vegetation cover and demographic composition occurred in many Dryland ecosystems. Such changes are expected to intensify in the coming decades, leading to significant consequences on carbon and energy budget, water resources, biodiversity, and wildfire risk (Allen et al., 2010; Breshears et al., 2005; Brodribb et al., 2020; Kulmatiski et al., 2020). To better predict the regional and global impact of Dryland ecosystems in response to climate change, it is crucial to quantify how hydroclimatic stresses regulate plant vulnerability and ecosystem fluxes (Bjorkman et al., 2018; Sperry and Love, 2015).

Plant responses to stress ultimately depend on the interplay of plant traits with the combination of soil and atmospheric stresses, which results from plant hydraulic processes (Sperry and Love, 2015; McDowell et al., 2019). As the soil dries down, declining leaf water potential (Ψ_l) could cause malfunctioning of xylem associated with cavitation, thus limiting water supply and possibly causing hydraulic failure. On the other hand, increasing atmospheric water demand, i.e., vapor pressure deficit (VPD), can modulate Ψ_l and restrict stomatal opening to prevent excessive water loss at the cost of restrained carbon gain. Therefore, the sensitivity of leaf water potential to water stresses (i.e., hydraulic

* Corresponding author.
E-mail address: hjp@lzu.edu.cn (J. Huang).

https://doi.org/10.1016/j.agrformet.2021.108701
Received 4 June 2021; Received in revised form 9 October 2021; Accepted 22 October 2021
Available online 29 October 2021

sensitivities) lies at the center of plant stress-responses. Besides, dozens of studies have demonstrated that stomata respond to Ψ_l directly (Anderegg and Venturas, 2020; Brodribb et al., 2003; Klein and Niu, 2014). However, many of the current ecosystem and land surface models still use empirical soil water stress functions to shut down stomata as soil water stress intensifies (Hu et al., 2009; Oleson et al., 2010; Sellers et al., 1996; Shuttleworth and Wallace, 1985). Doing so may overestimate the sensitivity of ecosystem flux to soil water stress (Liu et al., 2020b). Alternatively, plant hydraulics mechanistically describes plant water transport through the vascular system, assessing leaf water potential that directly regulates stomatal conductance (McDowell et al., 2019). Multiple studies have shown that incorporating plant hydraulics into the current theoretical framework of the soil-plant-atmosphere continuum better captures ecosystem water use especially under dry conditions (Anderegg et al., 2017; Bonan et al., 2014; Liu et al., 2020b; Mirfenderesgi et al., 2016). Testing the performance of the plant hydraulic model in Dryland ecosystems will thus facilitate a better understanding of the dynamics of plant hydraulic sensitivity and water and carbon fluxes under future water stress scenarios.

Declining leaf water potential under water stress reduces transpiration and photosynthesis while increasing mortality risk. Similar to hydraulic sensitivity, the extent to which mortality risk and ecosystem water flux change may also vary across the soil and atmospheric stress regimes. Recent studies suggest that VPD is projected to continue increasing throughout this century with elevated temperature (Ficklin and Novick, 2017; Yuan et al., 2019); whereas the projected change of soil moisture varies by geographic location with larger uncertainty, with diverse trajectories for tropical, subtropical, and temperate Drylands (Schlaepfer et al., 2017; Zhou et al., 2021). It is thus crucial to investigate the individual and combined impact of soil and atmospheric water stresses on mortality risk and ecosystem water flux in Dryland ecosystems. Besides, limited water flux has often been considered to be associated with increased ecosystem susceptibility under stress, such as in land surface models where both are directly linked to environmental stress through empirical relations per plant functional type (Niu et al., 2011; Oleson et al., 2010). However, a recent study on temperate forests in California suggested that the response trajectories of ecosystem water flux and vulnerability may not always be coupled under varying environmental conditions (Feng et al., 2017). What remains under-explored is under what soil and atmospheric water stresses the ecosystem water flux is or is not coupled with the ecosystem vulnerability to water stresses, especially in Dryland ecosystems.

Here, we systematically evaluated how hydraulic sensitivities, mortality risk, and evapotranspiration (ET) respond to soil and atmospheric water stresses. We focused on desert riparian species, which compose the most diverse and productive ecosystem in dryland deserts. The riparian species have crucial impacts on desert ecosystem functions including water use, productivity, ecosystem stability, and biodiversity (Stromberg et al., 2013; Wu et al., 2019), which are primarily controlled by water stresses. Desert riparian ecosystems are exposed to large seasonal variations of atmospheric water demand and seasonally shallow groundwater due to interaction with the water table in the river. The strong control and large variation in water stresses make the desert riparian ecosystem an ideal setting to evaluate plant hydraulic behaviors across stress regimes. Besides, desert riparian species include a collection of distinct hydraulic and morphological traits that generate different strategies to operate under water stresses (Brouillette et al., 2014; Zhang et al., 2017). Here we analyzed two typical desert riparian species with distinct traits, i.e., *Populus euphratica* and *Tamarix ramosissima*. Doing so allows investigation of the interaction between traits and stress regimes on the vulnerability and water use of desert riparian ecosystems. We used a plant hydraulic model (PHM) to describe plant hydraulic dynamics and ecosystem water flux under varying hydroclimatic conditions. The PHM was adapted from a recent study across multiple climate regions (Liu et al., 2020b) to account for the specific environmental settings of the desert riparian ecosystem. Because plant hydraulic traits strongly control stress-responses of desert riparian species (Zhang et al., 2017), it is important to appropriately parameterize the PHM. To do so, we used a model-data fusion approach to estimate the most likely hydraulic traits related to the plant water transport system (Liu et al., 2020b). The model was tested against the observed leaf water potential, sap-flow, and ecosystem ET. The optimized model was then used to estimate hydraulic sensitivity, mortality risk, and ET under a range of simulated stress scenarios. The analysis provides a diagnostic tool to assess ecosystem function in response to water stresses, which will facilitate water resources and ecosystem management under future climate.

2. Materials and methods

2.1. Plant hydraulic model

We used a plant hydraulic model (PHM) adapted from Liu et al. (2020b) to describe dynamic root water uptake, plant water potentials, stomatal operation, and transpiration. In the PHM, water extracted from the soil is transported through the xylem to the leaves following a water potential gradient from the roots to the leaves (Fig. 1a). Soil evaporation is calculated using the Penman-Monteith equation (Shuttleworth and Wallace, 1985; Song et al., 2018, 2020). Soil water is extracted from the soil into the roots, transported to the leaves through the xylem system, and dissipates into the atmosphere through the stomata. We assume continuity from the xylem in the roots all the way up to the xylem in the leaves. Thus, both xylem and leaf water potentials are determined by the dynamic budget of water supply from the root water uptake and atmospheric water demand, which in turn are controlled by soil moisture and VPD. The representation of root water uptake is adapted specifically for desert riparian trees described as follows. The rooting zone is discretized as four layers according to the soil texture measurements (Li et al., 2019a): a shallow-soil layer (0–30 cm), a middle-soil layer (30–100 cm), a deep soil layer (100cm-GWT), and a groundwater layer (GWT to the maximum rooting depth). In each layer, water is extracted by the roots following:

$$V_i = g_{sr,i}\left(\Psi_{s,i} - \Psi_r\right) \tag{1}$$

where V_i (mol m^{-2} s^{-1}) is the water uptake in the ith layer ($i \in \{1, 2, 3, 4\}$); $g_{sr,i}$ (mol m^{-2} s^{-1}) is the soil-root conductance in the ith layer; $\Psi_{s,i}$ (MPa) is the soil water potential in the ith layer, calculated using measured moisture content based on empirical soil-water relations (Clapp and Hornberger, 1978); and Ψ_r (MPa) is the root water potential.

The soil-root conductance has often been considered to be limited by soil hydraulic conductivity in unsaturated soils (Katul et al., 2003; Liu et al., 2020b). However, in the desert riparian ecosystem, when the groundwater level rises into the rooting zone, roots can access water in saturated soil. In this case, the soil-root conductance may no longer be limited by the high soil hydraulic conductivity, rather, by the maximum root conductance that is intrinsically determined by the radial and axial hydraulic structure of the root (North and Peterson, 2005; Rieger and Litvin, 1999). Therefore, to account for limitations of both the soil and the root, the soil-root conductance is represented using a cylindrical root model (Katul et al., 2003) capped by the maximum root conductance. That is,

$$g_{sr,i} = \begin{cases} \left(K_i\sqrt{RAI_i}\right) \Big/ \left(Z_{ri}\pi\rho_w g\right) & if\ g_{sr,i} < g_{r,\max} \\ g_{r,\max} & if\ g_{sr,i} \geq g_{r,\max} \end{cases} \tag{2}$$

where K_i (m s^{-1}) is the unsaturated soil hydraulic conductivity in the ith layer, calculated according to Darcy's law for unsaturated flow; RAI_i (m^2 m^{-2}) is the root area index the ith layer; $Z_{r,i}$ (m) is the depth of the ith layer; ρ_w (Kg m^{-3}) is the water density; g (m s^{-2}) is the gravitational acceleration; and $g_{r,\max}$ (m s^{-1} MPa^{-1}) is the maximum root conductance. The upper limit of soil-root conductance, i.e., $g_{r,\max}$, allows better

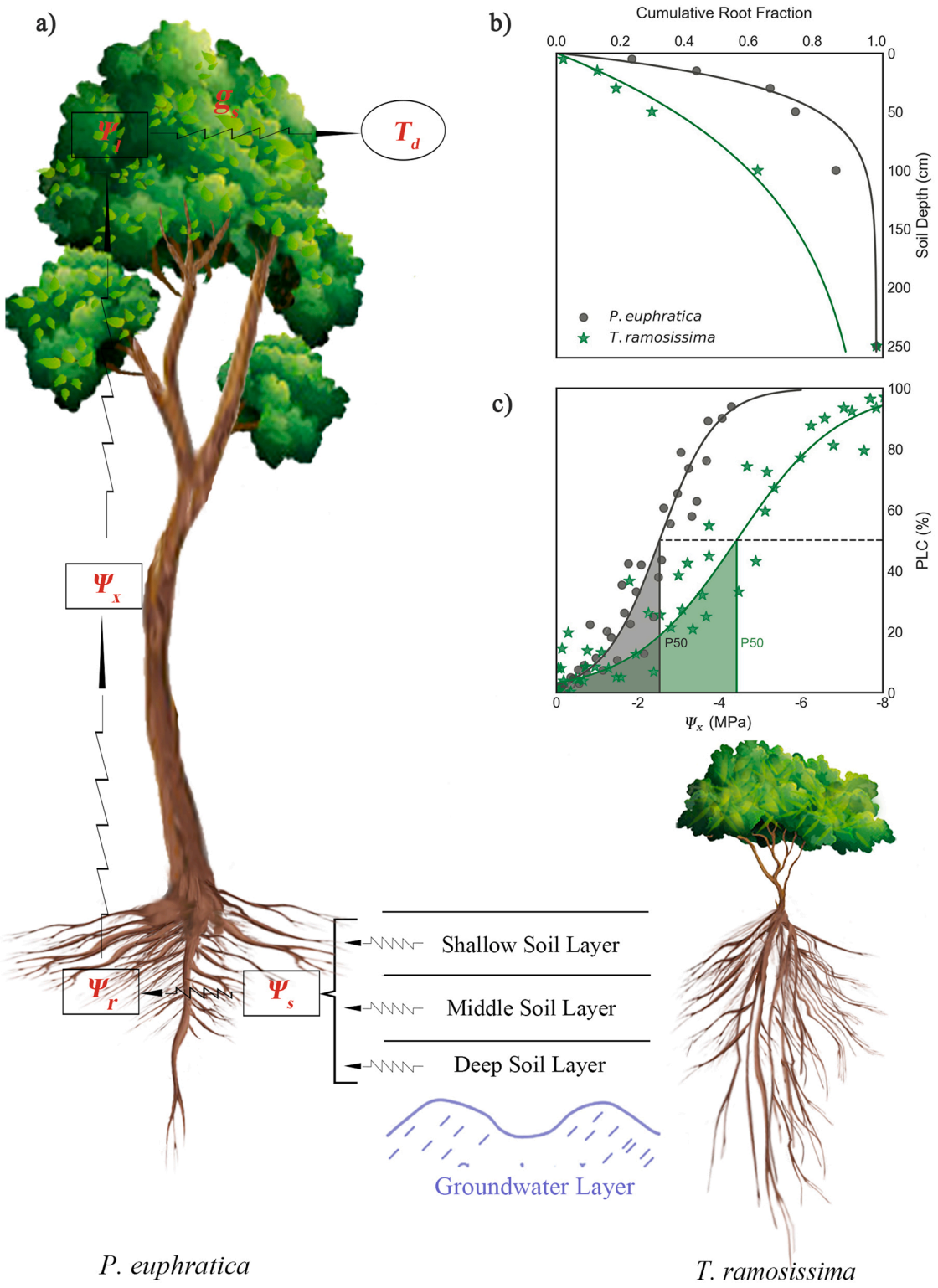

Fig. 1. Plant water transport system and key hydraulic traits of the two desert riparian species. (a) Model diagram describing water flow throughout the plant, where Ψ_s, Ψ_r, Ψ_x and Ψ_l represent water potentials in the soil, root, xylem and leaf; g_s is the leaf stomatal conductance, and T_d is transpiration. Soil profile is divided into the shallow, middle, deep soil layers and a groundwater layer. (b) Rooting profiles of *P. euphratica* (grey line) and *T. ramosissima* (green line). (c) Vulnerability curves of *P. euphratica* (grey line) and *T. ramosissima* (green line). P50 is the water potential corresponding to 50% loss of hydraulic conductivity (PLC).

characterization of root water uptake from the groundwater layer or soil layers close to saturation.

The total water flux extracted from the soil ($T_s = \sum_i V_i$) is transported through the xylem as follows (Sperry et al., 2017):

$$T_s = \int_{\Psi_r}^{\Psi_l} g_p(x)\mathrm{d}x \quad (3)$$

where x (MPa) is water potential within the xylem at any given location

between the roots and the leaves; g_p (m s^{-1} MPa^{-1}) is the xylem conductance, which reduces with plant water potential following a vulnerability curve as below.

$$g_p(x) = g_{p,max}[1 + (x/P50)^a]^{-1} \quad (4)$$

where $g_{p,max}$ (m s^{-1} MPa^{-1}) is the maximum xylem conductance; a is the shape parameter of the vulnerability curve; P50 (MPa) is the xylem water potential at which 50% of maximum xylem conductance is lost.

The water supply (T_s, mol m^{-2} s^{-1}) is dissipated through transpiration (T_d, mol m^{-2} s^{-1}), which is calculated based on energy balance on the canopy surface, that is:

$$T_d = \frac{\Delta R_{nc} + P_0 C_p g_a \mathrm{VPD}}{\Delta \lambda_l + P_0 C_p g_a / G_S} \quad (5)$$

Where λ_l (J mol^{-1}) is the latent heat of vaporization of water; R_{nc} (J m^{-2} s^{-1}) is the net radiation (R_n, J m^{-2} s^{-1}) absorbed by the canopy, following Beer's law; P_0 (Pa) is the atmospheric pressure; Δ (Pa K^{-1}) is the rate of change of saturated vapor pressure with temperature; C_p (J mol^{-1} K^{-1}) is the specific heat of air; g_a (mol m^{-2} s^{-1}) is the aerodynamic conductance, following (Campbell and Norman, 2012); G_s (mol m^{-2} s^{-1}) is the canopy conductance, which is equal to $[g_a^{-1} + (g_s \mathrm{LAI})^{-1}]^{-1}$ (Bonan, 1996), where LAI (m^2 m^{-2}) is the leaf area index and g_s (mol m^{-2} s^{-1}) is the stomatal conductance at the leaf level. Here, g_s is calculated based on the leaf-gas exchange optimality theory (Katul et al., 2009):

$$g_s = \mathrm{argmax}(f_c(g_s) - \lambda f_e(g_s)) \quad (6)$$

where f_c (g_s) and f_e (g_s) are the water loss and carbon fixation respectively; λ (μmol mol^{-1}) is the marginal water use efficiency. In the plant hydraulic system, g_s can be solved under a given λ by combining Eq. (6) with the biochemical demand for CO_2 (Farquhar et al., 1980). λ has been demonstrated to relate to Ψ_l (Manzoni et al., 2011), that is,

$$\lambda = \lambda_{ww} \exp(\beta_0 \overline{\Psi_l}) \quad (7)$$

where λ_{ww} (μmol mol^{-1}) is λ under the ambient CO_2 concentration and well-watered conditions; β_0 (MPa^{-1}) is the slope parameter; $\overline{\Psi_l}$ (MPa) is the mean Ψ_l in the previous day (Huang et al., 2017).

Assuming a resistance-based system with no capacitance and thus negligible plant water storage, leaf water potential and transpiration can be solved by equating the water supply (Eq. (3)) to the water demand (Eq. (5)).

2.2. Site properties and datasets

The PHM was applied to two desert riparian sites (1.5 km apart) of the Heihe Watershed Allied Telemetry Experimental Research (HiWATER, Li et al., 2017), which are located downstream of the Heihe river basin, Northwest China. The mean annual potential evaporation exceeds 3700 mm, whereas the mean annual precipitation is around 42 mm (Zhu et al., 2012). Mean temperatures in July and January are 26.95 and −11.68 °C, respectively (Yu et al., 2017). The two sites are each dominated by a common desert riparian species in China, *Populus euphratica* and *Tamarix ramosissima*, respectively (Ayup et al., 2015). The *P. euphratica* site (41.99 ° N, 101.13 ° E) and the *T. ramosissima* site (42.00 ° N, 101.14 ° E) are both located on a flood plain, approximately 1.0 km and 0.8 km from the riverbank, respectively.

The soil texture is silt loam in the shallow and middle layers, and sand in the deep and groundwater layers at both sites based on in situ samples (Li et al., 2019a). The *P. euphratica* has a mean age of 120 years and a mean canopy height of 13.2 m; whereas the *T. ramosissima* is 6 years old and 1.9 m high on average. The maximum rooting depth is 4 m and 5 m for *P. euphratica* and *T. ramosissima,* respectively (Bai et al., 2021). The vertical rooting profile was estimated by fitting the measured fine root biomass across the soil layers to a root distribution model (Jackson et al., 1997) (Fig. 1b). The hydraulic trait P50 was also measured using the benchtop dehydration method (Skelton et al., 2015) for the two species (Fig. 1c). A detailed description of these measurements can be found in Bai et al. (2021).

The model is driven by half-hourly meteorological and hydrological conditions measured at the sites, including net radiation, air temperature, humidity, precipitation, wind speed, sensible heat fluxes, friction velocity, the vertical profile of soil water content, and the depth to groundwater table (GWT, m). CO_2 and H_2O fluxes were monitored above the canopy using open-path eddy covariance measurements at each site. Soil water content (SWC, m^3 m^{-3}) was monitored at 4, 10, 20, 40, 80, 120, 160 and 200 cm. Values of SWC were averaged over the shallow (depths of 4, 10 and 20 cm), middle (depths of 40 and 80 cm) and deep (depths of 120, 160 and 200 cm) soil layers. The growing seasons, i.e., April to October, during 2014–2017 were used as the study period. Days with precipitation or daily minimum temperature below 0 °C were excluded from the analysis. Hydro-meteorological data is publicly and freely downloadable from Figshare (https://doi.org/10.6084/m9.figshare.c.3706849). Data collection was described in Li et al. (2017). Besides, leaf water potentials at the predawn (Ψ_{pd}, between 5 am and 6 am) and at the midday (Ψ_{md}, between 12 am and 1 pm) were measured on twigs of five sample trees across the growing season in 2016 (Li et al., 2019a), a total of 50 samples in five months. Transpiration of the *P. euphratica* during the 2014 and 2015 growing seasons was measured using the thermal dissipation sap flow velocity probes (Bai et al., 2017). The leaf area index (LAI) at each site was extracted from the MODIS (Moderate Resolution Imaging Spectroradiometer) product (MCD15A3H.006) with a spatial and temporal resolution of 500 m and 4 days. LAI was filtered using the Savitzky-Golay filter to diminish noise and then linearly interpolated to the same temporal resolution as the flux measurements.

2.3. Estimating hydraulic traits using MCMC

Evaluating plant hydraulic response to water stresses using the PHM requires appropriate parameterization of plant hydraulic traits. Here, the model parameters related to the plant water transport system were systematically estimated in a Bayesian framework using Markov chain Monte Carlo (MCMC). This approach identifies the most likely set of traits that leads to model outputs consistent with observed constraints at each site, while also providing estimates of parameter uncertainty. Six plant hydraulic traits (λ_{ww}, β_0, P50, a, $g_{p,max}$, and $g_{r,max}$) were jointly estimated using MCMC. Specifically, an adaptive Metropolized independence sampler was used to generate posterior samples (Ji and Schmidler, 2013). This sampling method has been used to effectively retrieve plant hydraulic traits at multiple flux tower sites (Liu et al., 2020b). Prior information of physiologically realistic ranges and constraints on hydraulic traits in Liu et al. (2020b) were also used here. For the additional trait $g_{r,max}$, a non-informative prior spawning 5×10^{-9} to 5×10^{-5} m s^{-1} MPa^{-1} (flat in a log scale) was used, which covers the range of estimated values in measurement studies (Rieger and Litvin, 1999).

The MCMC was constrained by both the observed ET and the leaf water potential, which are directly regulated by plant hydraulic traits. ET observations in three (2014–2016) out of the four years and all available leaf water potential observations were used to estimate the parameters. The posterior distribution of hydraulic traits was estimated based on the product of the prior and the likelihood function. The likelihood function was calculated by comparing the modeled Ψ_l and ET with observations. For each category of Ψ_l and ET, the errors between the model output and observation were considered independently and identically distributed, following a zero-mean Gaussian distribution with an unknown variance to be estimated. The total likelihood was then calculated as the summation of the likelihood of Ψ_l and ET, that is,

$$\log\left(L\left(y_e^{1:n_e}, y_p^{1:n_p}\middle|\theta\right)\right) = \sum_{i=1}^{n_e}\log L\left(y_e^i|\theta\right) + \sum_{j=1}^{n_p}\log L\left(y_p^j\middle|\theta\right)\right) \quad (8)$$

where L is the likelihood of observed ET (y_e) and Ψ_l (y_p) under given parameters (θ, i.e., the six hydraulic traits); n_e and n_p are the number of valid data of ET and Ψ_l, respectively. y_e^i is the ith observation of ET; y_p^j is the jth observation of Ψ_l; $y_e^{1:n_e}$ and $y_p^{1:n_p}$ are the collection of all observed ET and Ψ_l, respectively.

Ten independent MCMC chains, each with a random starting point, were used for each site. Within- and among-chain convergences were diagnosed by the Geweke (< 1.05) and Gelman-Rubin values (< 0.2) (Brooks and Gelman, 1998). All MCMC chains converged before 11,000 steps. The samples after convergence provided the estimation of the joint posterior distribution of the target parameters. Among the posterior samples, 100 sets of parameters were randomly selected and their average values were used for the analysis below.

2.4. Model assessment

The PHM was run at a half-hourly timestep. The modeled outputs were compared to three measured datasets, including the predawn and midday leaf water potentials (Ψ_l) of both species during the 2016 growing season, the daily sap-flow-based transpiration (T_d) of *P. euphratica* in the growing seasons of 2014 and 2015, and the daily ecosystem evapotranspiration (ET, mol m^{-2} s^{-1}) from 2014 to 2017. The unit was converted to mm d^{-1} based on the molecular mass and density of H_2O when compared to measurements. Note that the model was constrained by ET in the first three years (2014 to 2016) and leaf water potential during the 2016 growing season. ET in the last year (2017) and all transpiration observations (2014–2015) were not used as constraints, thus providing test sets to evaluate the predictive performance of the model. The accuracies of T_d, as well as the training and test sets of ET, were estimated using the coefficient of determination (R^2) and the root mean square error (RMSE).

2.5. Scenario analysis

We used the optimally parameterized PHM to evaluate the ecophysiological response to water stress. Specifically, we focused on three variables, hydraulic sensitivity, tree mortality risk, and ET.

Temporal variation in Ψ_l is influenced by both soil water and VPD (Anderegg et al., 2017). The hydraulic sensitivity to soil water stress (σ_{soil}) was calculated according to Martínez-Vilalta et al. (2014):

$$\Psi_{md} = \sigma_{soil}\Psi_{pd} + \Lambda_s \quad (9)$$

where Ψ_{pd} and Ψ_{md} are the predawn and midday Ψ_l across the growing seasons; Λ_s is the intercept. Likewise, based on the linear relationship between the midday VPD and Ψ_{md} (Fig. S3), we also quantified the hydraulic sensitivity to atmospheric water stress (σ_{air}) using the following regression:

$$\Psi_{md} = -\sigma_{air}\mathrm{VPD}_{md} + \Lambda_a \quad (10)$$

where VPD_{md} is the midday vapor pressure deficit across the growing seasons; and Λ_a is the corresponding intercept. Here, a negative sign was added in front of σ_{air} because unlike the positively related Ψ_{md} and Ψ_{pd} in Eq. (9), Ψ_{md} and VPD_{md} are often negatively related. The negative sign ensures a positive σ_{air} comparable to σ_{soil}.

We also investigated stress-induced mortality risk using modeled leaf water potential and stomatal conductance. The duration plants operate under high percentage loss of conductivity can be used to distinguish tree mortality (Liu et al., 2017; Mcdowell et al., 2013; Sperry et al., 2015). Here, two types of duration-based tree mortality risk, i.e., hydraulic failure risk (HFR) and stomatal closure risk (SCR) were estimated under dynamic atmospheric and soil water stresses. HFR quantifies the fraction of days when the daily minimum leaf water potential falls below P50 (HFR=hours (Ψ_x<P50)/hours of the entire record), and SCR was formulated as the fraction of days on which stomata are completely closed (SCR=hours ($g_s <= 0$)/hours of the entire record). Both HFR and SCR are based on the duration of stressed physiological states, which are arguably more effective in capturing tree mortality than intensity-based metrics (Mcdowell et al., 2013; Sperry and Love, 2015). The same risk metrics have also been used to evaluate changes in mortality risk under different climate scenarios (Liu et al., 2017).

Based on the optimized model at both sites, a systematic scenario analysis was used to estimate the response of hydraulic sensitivities, stress-induced mortality risks, and ET to a range of atmospheric and soil water stress scenarios. In each stress scenario, atmospheric and soil water stresses were manually changed to generate different combinations of stress scenarios. The observed time series of atmospheric water stress (i.e., VPD) was multiplied by a factor ranging from 20 to 200% with a step size of 10%. Scenarios of soil water stress were generated by adding a uniform change, from +0.4 to −2.0 m with a step size of 0.1 m, to the observed time series of GWT. The highest increase of GWT (+0.4 m) was used because an increase higher than 0.4 m will cause GWT to rise above the ground surface. Note that soil moisture also changes with GWT. To account for the nonlinear variation of soil moisture with GWT, we derived piecewise linear relationships between GWT and soil moisture of each layer based on observations (Figs. S1, S2). The derived relations were used to represent soil moisture across layers as the GWT varies. Detailed information on calculations of soil water content under new GWT scenarios is available in Supplementary Note S1 and S2. In this way, the generated stress scenarios preserve the observed seasonal and inter-annual fluctuations as well as empirical relations among hydroclimatic conditions. The designed 500 combinations of VPD and GWT were then used to drive the hydraulic model parameterized with 100 sets of posterior parameters. The 100 ensembles were used to investigate the hydraulic sensitivities, mortality risks and ET of the studied ecosystems. The notations and units of variables used throughout are listed in Table S1.

3. Results

3.1. Parameter retrieval using model-data fusion

The model-data fusion approach identifies the root, xylem and leaf hydraulic traits of the two studied species (Fig. 2). For both species, xylem hydraulic parameters (i.e. $g_{p,\max}$, P50 and a) are widely distributed over the prior ranges (Fig. 2b–d), which suggests a low sensitivity of the likelihood function (Eqn. (8)) to the xylem traits. However, the stomatal (i.e. λ_{ww}, β_0) and root (i.e. $g_{r,\max}$) hydraulic traits exhibit narrow posterior distributions, indicating strong controls on ET and leaf water potential used as constraints. The low sensitivity to the xylem traits is consistent with findings at multiple FLUXNET sites (Liu et al., 2020b) and a remote sensing scale (Liu et al., 2020a) likely due to leaf water potential usually being much higher than P50 and thus rarely influenced by P50. The low sensitivity to the xylem traits is also affected by the correlation of P50 with other hydraulic traits across MCMC samples that generate similar model likelihoods. In addition, under sufficient water supply, the tree species (*P. euphratica*) has a higher maximum root conductance ($g_{r,\max}$) and marginal water use efficiency (λ_{ww}), than the shrub species (*T. ramosissima*) (Fig. 2a, e); and *T. ramosissima* exhibits a stronger stomatal control as leaf water potential declines (more negative β_0, Fig. 2f).

3.2. Model performance in estimating Ψ_l, T and ET

The performance of the PHM was assessed by comparing measured leaf water potentials, sap flow, and ecosystem-scale ET with model outputs. Specifically, the PHM captures both the diurnal range and seasonal variations of measured Ψ_l for both species (Fig. 3). Notably,

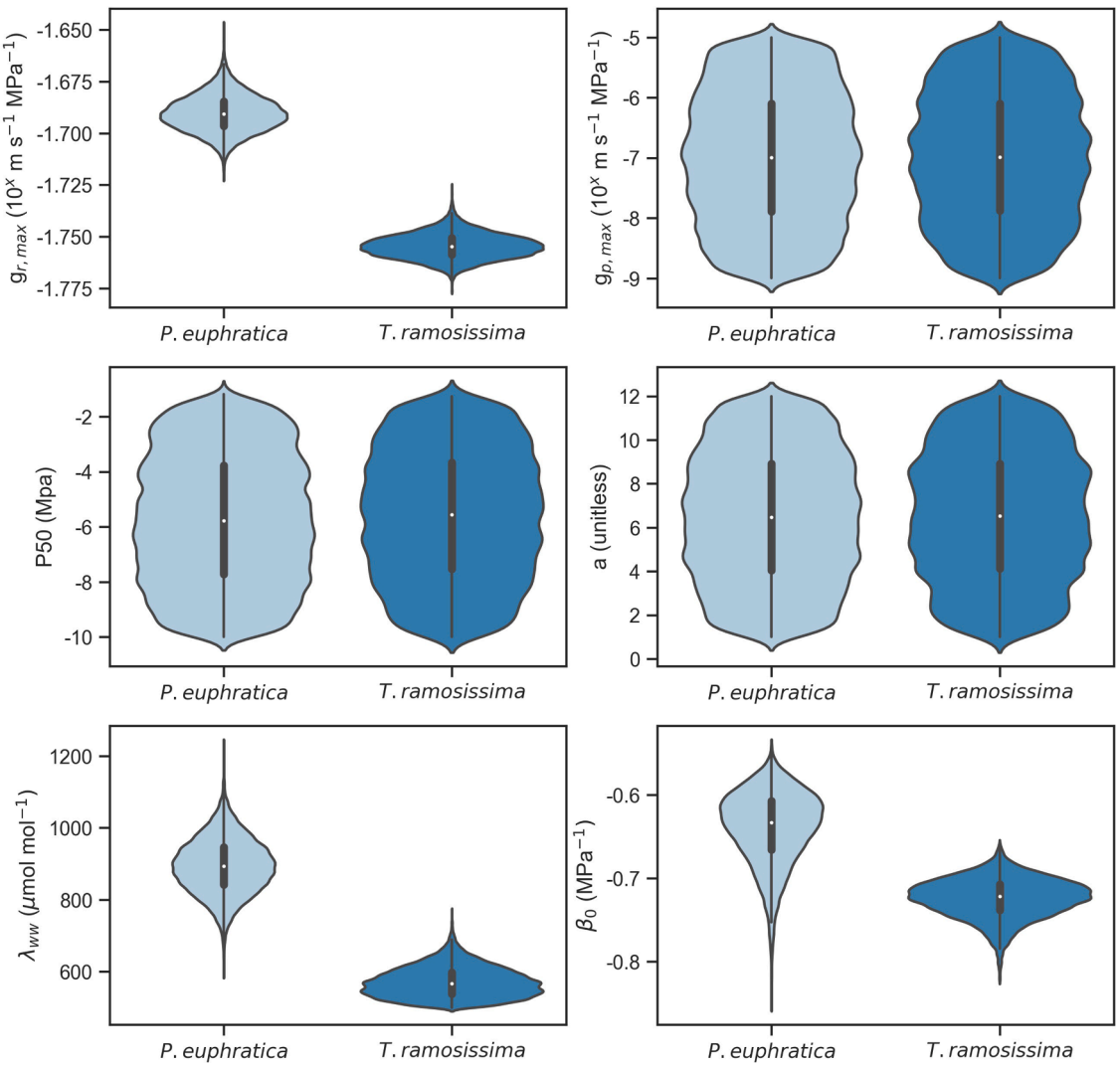

Fig. 2. Posterior distributions of hydraulics parameters. $g_{r,\max}$ is the maximum root conductance; $g_{p,\max}$ is the maximum whole-plant xylem conductance; P50 is the water potential corresponding to the 50% loss of hydraulic conductivity; a is the curvature parameter of the vulnerability curve; λ_{ww} is the marginal water use efficiency under the ambient CO_2 concentration and well-watered conditions; and β_0 is the sensitivity parameter of the marginal water use efficiency. The white dot in each violin represents the median; the black box and bar represent the mid-50% range and the full range, respectively.

although transpiration was not included as a model constraint, the modeled transpiration reproduced the observation based on the sap flow of *P. euphratica*, with R^2 of 0.64 and RMSE of 0.47 mmol m^{-2} s^{-1} (Fig. 4). At an ecosystem scale, the PHM was able to capture ET within both the training and the test sets (Fig. 5), with R^2 of 0.76 and 0.79 respectively at the *P. euphratica* site, and 0.69 and 0.78 at the *T. ramosissima* site. The training and predictive performance of PHM in estimating the described hydraulic states and fluxes at diurnal (Fig. 3), seasonal and inter-annual scales (Figs. 4, 5) support its ability to properly describe plant hydraulic responses of the two studied species to hydroclimatic variations.

3.3. Variation in hydraulic sensitivities across stress scenarios

We systematically analyzed the sensitivities of leaf water potential to soil (σ_{soil}) and atmospheric (σ_{air}) water stresses, referred as hydraulic sensitivities hereafter (Fig. 6). Instead of being a species-specific trait that remains relatively constant, the hydraulic sensitivities of both species vary significantly across stress regimes. Under the current observed stress conditions, σ_{soil} of both species is greater than 1 (OBS in Fig. 6), indicating leaf water potential drops at a higher rate than soil water potential does during soil dry-down. However, as the stress intensifies (moving toward the upper right corner of Fig. 6a, b), the sensitivity to soil stress declines. The sensitivity to VPD (σ_{air}) also shows similar patterns as σ_{soil}, although its variation across stress regimes is dominated by VPD (Fig. 6c, d). The reduced sensitivities to both soil and atmospheric stresses indicate that leaf water potential becomes decoupled to stresses under severe conditions. However, the extent to which the hydraulic status decouples from given external stress varies across species. For example, as GWT drops by 2 m, σ_{soil} reduces from 1.58 to 0.82 for *P. euphratica* but remained almost the same (1.38 to 1.26) for *T. ramosissima*.

3.4. Response of mortality risk to water stresses

We used modeled leaf water potential and stomatal conductance to estimate stress-induced mortality risk, including hydraulic failure risk (HFR) and stomatal closure risk (SCR), under the same stress scenarios as in Fig. 6. The results suggest that both the magnitude of HFR and SCR and their sensitivities to stresses significantly vary across stress regimes (Fig. 7). For both species, SCR increases as GWT declines and as VPD increases, due to the limitation of leaf water potential and VPD on stomatal opening (Fig. 7a, b). Remarkably, SCR increases faster with stress under severe stress scenarios (upper right corner of Fig. 7a, b) than under low stress scenarios (lower left corner of Fig. 7a, b). For example,

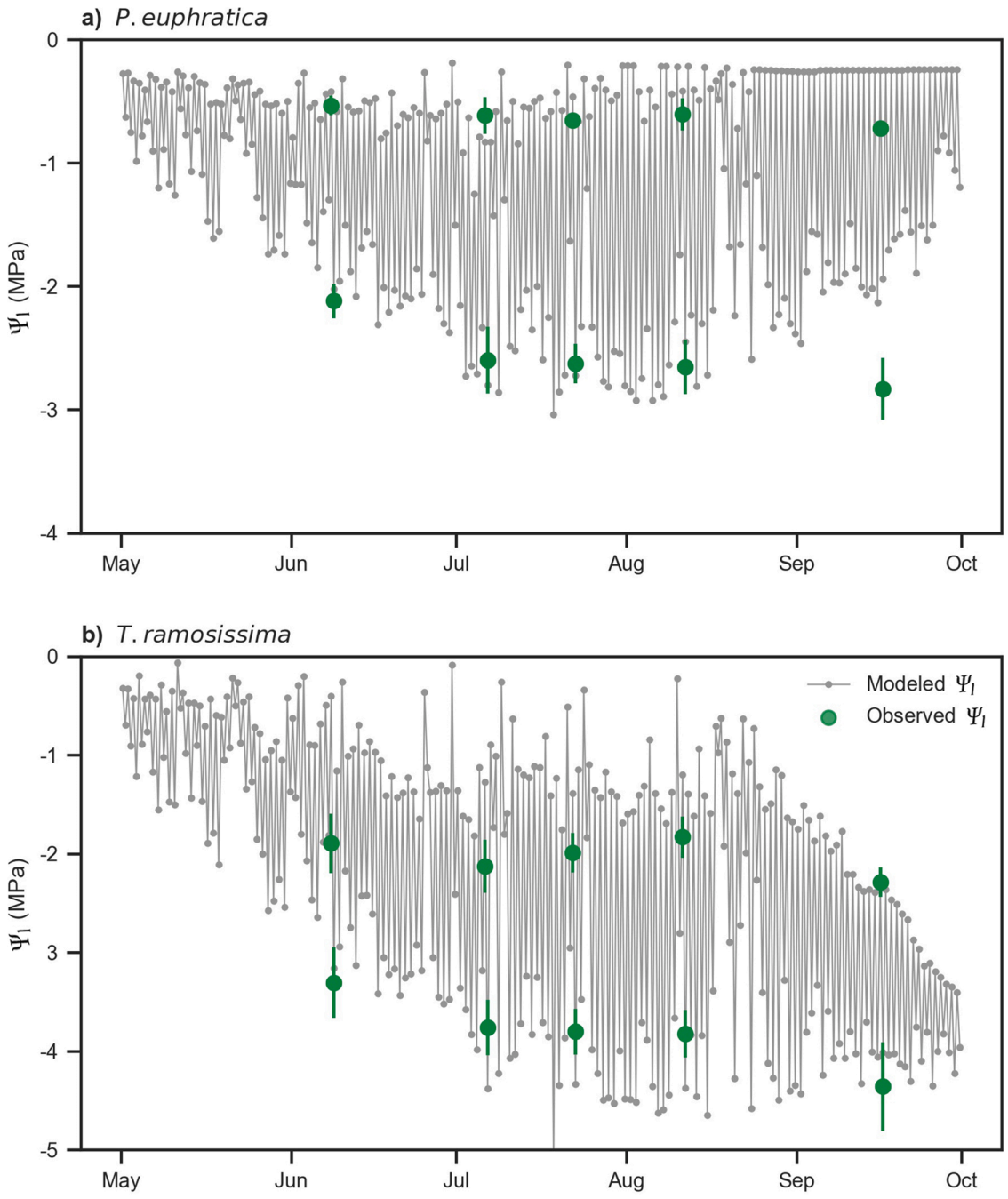

Fig. 3. Modeled and observed leaf water potentials (Ψ_l) of *P. euphratica* and *T. ramosissima* during the growing season of 2016. Grey dotted lines represent the modeled Ψ_l. The green dots denote the observed Ψ_l. The vertical green bars denote uncertainty ranges of the measured Ψ_l.

under current GWT (OBS in Fig. 7a, b), 40% increase of VPD only increases SCR by less than 5% for both species. However, when GWT drops by −1.4 m, the same increase of VPD would cause 36% and 12% increase of SCR for *P. euphratica* and *T. ramosissima*, respectively. This result highlights the compound impact of soil and atmospheric stresses on mortality risk. HFR, on the other hand, mainly increases with decreasing GWT due to reduced leaf water potential (Fig. 7c, d). Starting from VPD conditions lower than the current observed scenario, increasing VPD intensifies HFR through reduced leaf water potential, which creates a sufficient potential gradient for water supply to meet the increased demand of ET. When VPD exceeds the current observed scenario, its limitation on stomatal conductance attenuates water demand and therefore decreases HFR. As a result, HFR remains stable or even reduces with increasing VPD under a high VPD condition. Similar to SCR, HFR also increases faster under severe soil stress scenarios, but not under increased atmospheric stress scenarios. Specifically, under the observed stress scenario (OBS in Fig. 7c, d), 0.4 m decline of GWT only intensifies HFR of both species by less than 5%; while under a scenario where GWT is already 1.0 m lower than the observation, the same 0.4 m decline of GWT would dramatically increase HFR by 22% and 13% for *P. euphratica* and *T. ramosissima*, respectively. Under most stress scenarios, *T. ramosissima* exhibits lower risk magnitude and stress sensitivities than *P. euphratica* (Fig. 7b, d), indicating a stronger drought resistance of *T. ramosissima*.

3.5. Response of et to water stresses

The scenario analysis was also used to estimate the response of T_d

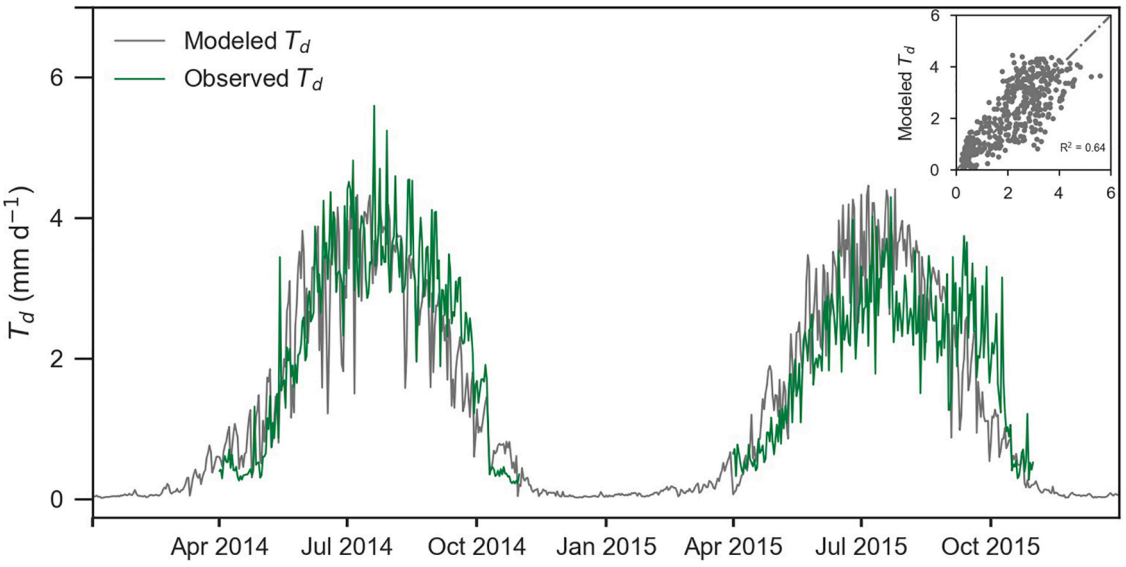

Fig. 4. Comparison between modeled (grey line) and measured (green line) daily transpiration (T_d) of *P. euphratica* during the growing seasons of 2014 and 2015.

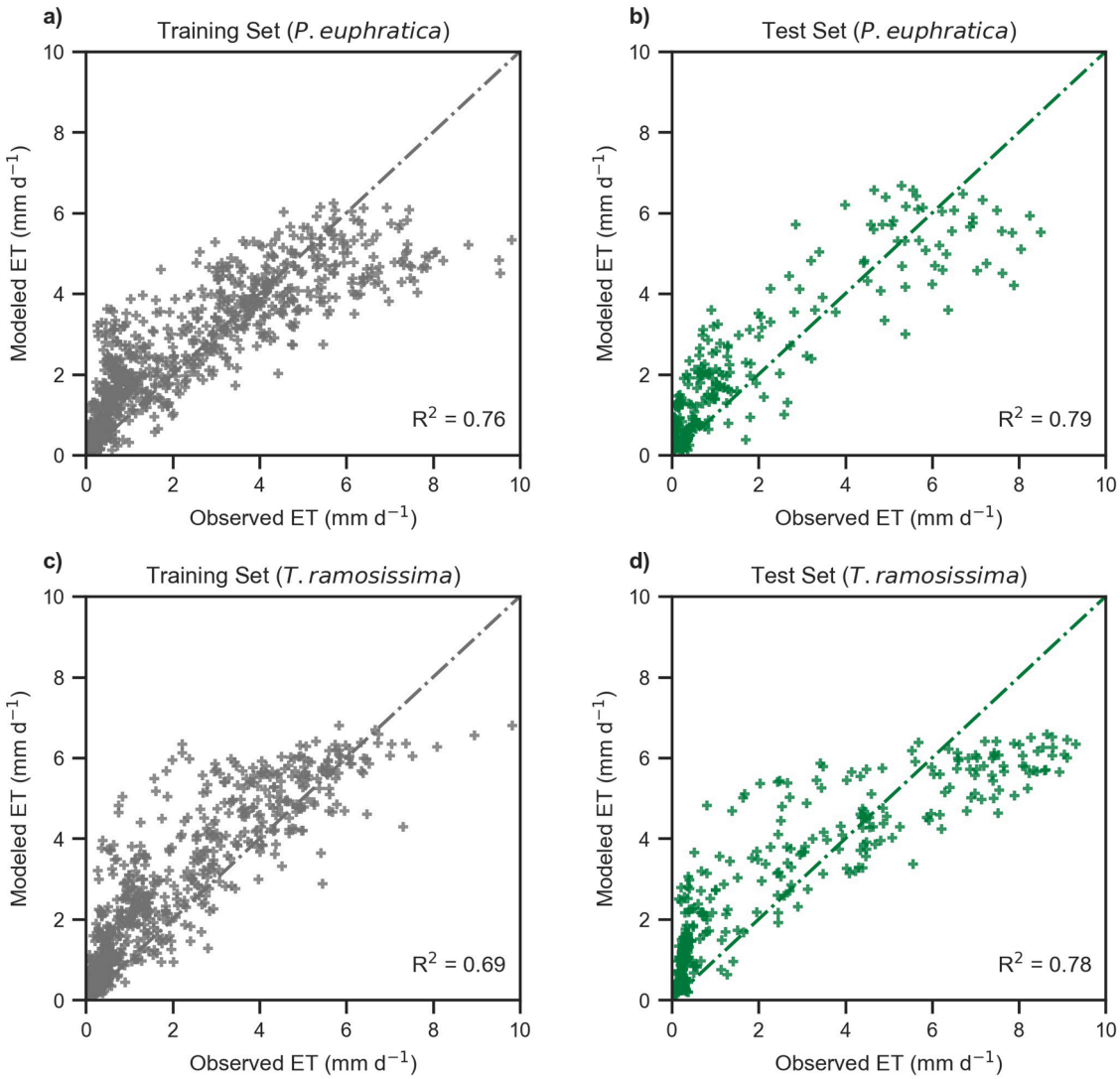

Fig. 5. Model performance in estimating observed daily evapotranspiration (ET) over the (a, c) training and (b, d) test period at the (a, b) *P. euphratica* and the (c, d) *T. ramosissima* sites.

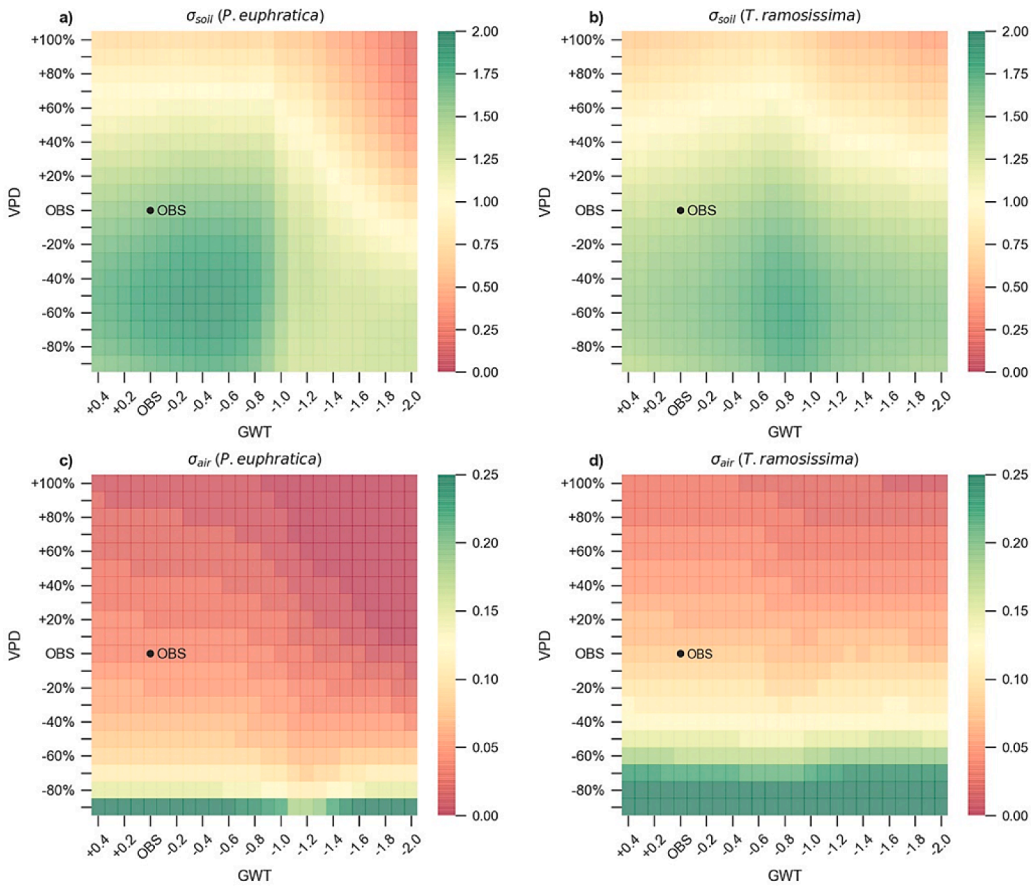

Fig. 6. Sensitivities of leaf water potential to soil (σ_{soil}) and atmospheric (σ_{air}) water stresses across stress regimes of average groundwater table (GWT) and VPD for the two studies species. OBS denotes the current observed stress scenario.

(Fig. S4) and ET (Fig. 8) to water stresses. Both T_d and ET show similar responses to dynamic soil and atmospheric water stresses. Specifically, ET reduces as GWT declines, though with varying sensitivities across stress regimes. At the *P. euphratica* site (Fig. 8a), reducing GWT barely limits ET under low stress scenarios (low VPD and high GWT), as suggested by nearly horizontal contour lines in the lower left corner of Fig. 8a. However, under moderate to high VPD conditions, ET quickly reduces with declining GWT. For example, starting from the observed stress status, 1 m decline of GWT would only cause 15% decrease of ET. However, additional 1 m decline of GWT (to 2 m below the current status) would cause a much higher additional decrease of 35%. Under VPD conditions lower than −40%, ET increases are mainly dominated by VPD. Nonetheless, as extremely high VPD limits stomatal conductance, ET remains relatively constant or even slightly reduces with increasing VPD, which is demonstrated by the nearly vertical contour lines in the upper right corner of Fig. 8. This pattern suggests that ET is driven by atmospheric water demand under low stress conditions, while limited by soil water supply under high stress conditions. The red-dashed line in Fig. 8a denotes the ridge line of the contours of *P. euphratica*, which separates the stress domain to demand-driven (lower left) and supply-limited (upper right) regimes. As expected, the separation of demand-driven and supply-limited regimes varies with species properties. At the *T. ramosissima* site, ET is mostly demand-driven except when VPD becomes 60% higher than the observed scenario (Fig. 8b). ET of the *T. ramosissima* site is less sensitive to both soil and atmospheric water stresses compared to that of the *P. euphratica* site, which indicates a greater capability to buffer water stresses.

4. Discussion

4.1. A dynamic view of hydraulic sensitivity

Our study estimates the response surfaces of hydraulic sensitivities of two desert riparian species under different soil and atmospheric water stresses. Consistent with previous studies (Feng et al., 2017; Li et al., 2019b; Matheny et al., 2017; McLaughlin et al., 2017; Sperry and Hacke, 2002; Wu et al., 2021), our results also demonstrate that plant hydraulic sensitivities vary significantly with environmental stresses (Fig. 6). Notably, the systematic scenario analysis here reveals the direction of hydraulic sensitivity in response to stress. That is, from moderate to extreme water stress conditions, leaf water potential becomes less sensitive to stresses (the upper right parts of Fig. 6a and c). Under extreme water stresses, variation of Ψ_l drops to a minimal level and becomes decoupled from soil moisture or VPD. Such reduction of sensitivity occurs not only under dry soil, as reported in most previous studies (Feng et al., 2019; Guo et al., 2020; Hochberg et al., 2018; Tramontini et al., 2014), but also under dry atmosphere such as during heat waves (Trugman et al., 2018). As droughts are expected to become hotter under climate change (IPCC, 2013), evaluating the impact of the nonlinear hydraulic response to both soil and atmospheric moisture stresses become increasingly important. Given that more land surface models start to explicitly represent plant hydraulics, further study is needed to evaluate how dynamic hydraulic sensitivity affects water/-carbon fluxes and ecosystem vulnerability in a global change context.

4.2. Ecosystem vulnerability regulated by hydraulic traits

As a direct result of declining leaf water potential, mortality risk is

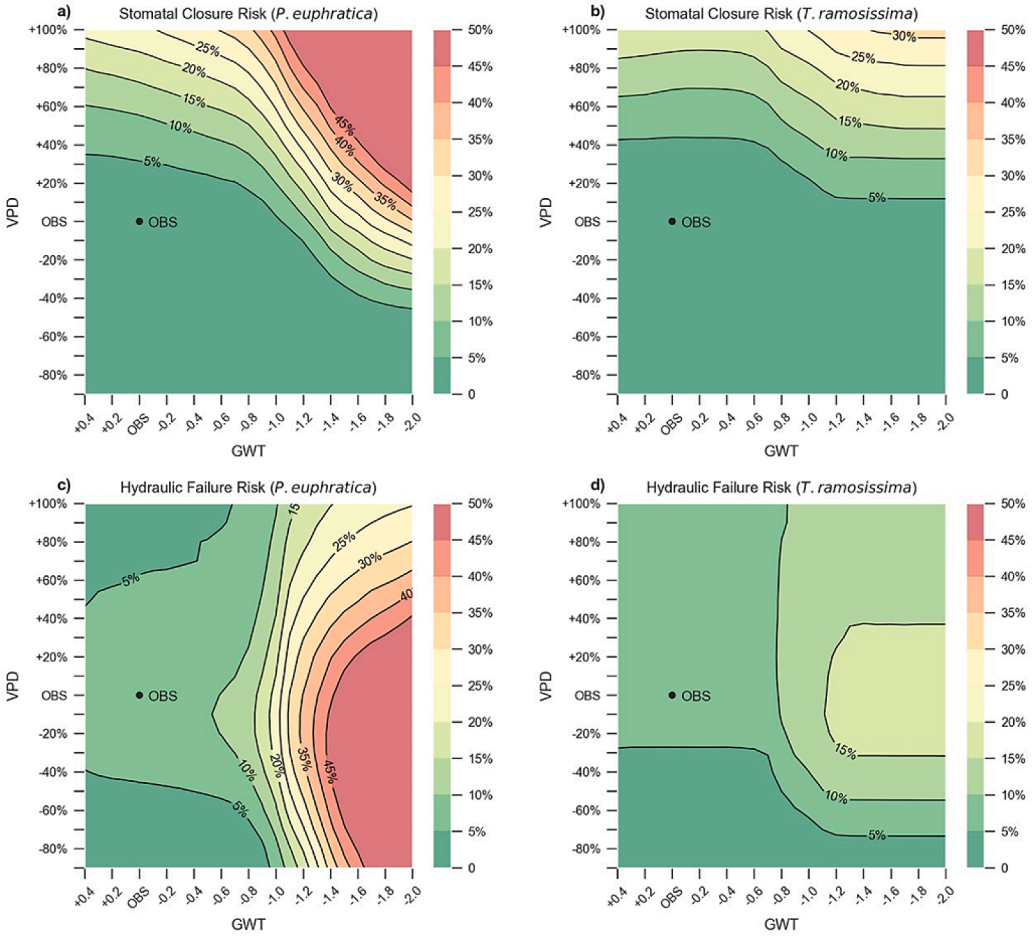

Fig. 7. Estimated stomatal closure risk (SCR) and hydraulic failure risk (HFR) across stress regimes of average groundwater table (GWT) and VPD for the two studies species. OBS denotes the current observed stress scenario.

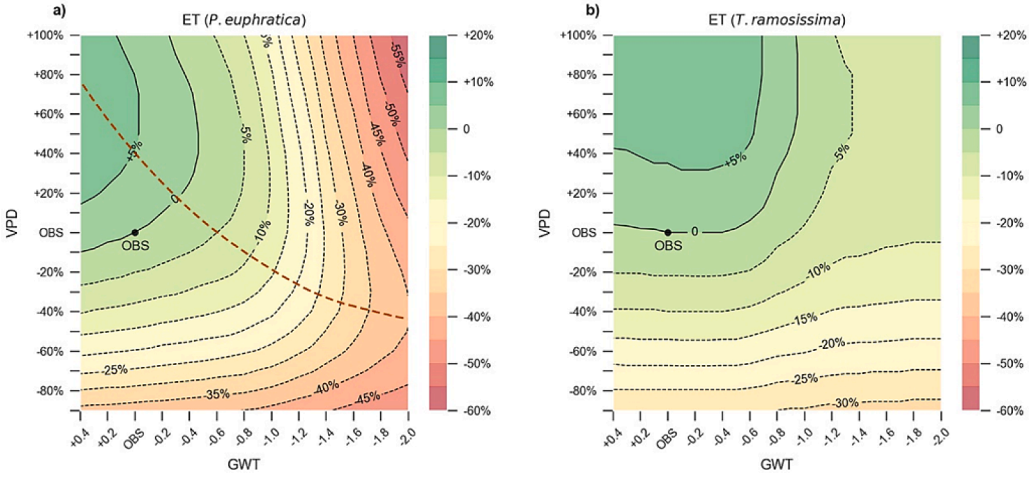

Fig. 8. Estimated evapotranspiration (ET) across stress regimes of average groundwater table (GWT) and VPD for the two studied species. OBS denotes the current observed stress scenario under dynamic soil and atmospheric water stresses. The red dashed line in (a) denotes the ridge line of the contour map.

intensified under compound soil and atmospheric water stresses (Feng et al., 2017). Comparing the two species, *T. ramosissima* shows lower hydraulic sensitivities and mortality risks than *P. euphratica* does under the same stress scenario (Figs. 6, 7). This result indicates *T. ramosissima* is more resistant to water stress. Previous studies suggested that taller trees tend to be more vulnerable to cavitation than shorter trees (Brodribb et al., 2020; McDowell and Allen, 2015). Here, *T. ramosissima* is much shorter and more drought-resistant. Note that the difference in drought resistance between the two species is unlikely caused merely by canopy height, as the difference of the maximum xylem conductance ($g_{p,\max}$, inversely related to canopy height) between the two species is statistically indistinguishable (Fig. 2b). *T. ramosissima* also has deeper roots and a greater proportion of deep roots (Fig. 1a, b), which allows access to deep groundwater when the soil dries out (Miller et al., 2010).

Besides, *T. ramosissima* also has a more negative P50 (Fig. 1c) and smaller xylem vessels, as reported by contemporary studies (Ayup et al., 2015; Bai et al., 2021), thereby preventing embolism and xylem cavitation under severe soil and atmospheric water stresses (Choat et al., 2018; Manzoni et al., 2014). Similar to a previous forest hydraulic model (Christoffersen et al., 2016), these characteristics also highlight hydraulic traits that play important roles in simulating the stress resistance of desert riparian ecosystems.

We used a simplified resistance-based scheme to represent plant water transport assuming no capacitance following previous studies (Katul et al., 2003; Manzoni et al., 2014). This simplification breaks the link between water pressure and storage, while it significantly reduces the computation load for effective estimation of plant hydraulic traits, which enables all the scenario analyses. Like in the previous studies, omitting capacitance and regardless of trait plasticity introduces uncertainties (Keenan and Niinemets, 2016; Mrad et al., 2018). Plant water storage is expected to buffer the decline of leaf water potential and thus introduce 'legacy effects' on the transpiration response to hydroclimatic stresses (Mrad et al., 2018). Due to the potential impact of plant water storage, the magnitude of mortality risk is expected to be lower, and ET is expected to be higher than the estimates here. However, the relative response patterns to different stress scenarios likely remain consistent. Besides, as plant water storage has been found to affect plant water use mainly at a diurnal scale (Huang et al., 2017), it is expected to marginally alter the main findings on stress-response patterns based annual averages of ET and mortality risk. In addition, re-occurring water stresses may alter the seasonal LAI and plant hydraulic traits (e.g., the leaf-specific hydraulic conductivity and the Huber value) (López et al., 2016; Klein et al., 2018), both of which was not considered here. Due to trait plasticity, recurring water stress could alter plant traits, e.g., reducing LAI increases the risk of carbon starvation, and partial refilling of the xylem prevents plants from full recovery after experiencing water stress, which impairs the hydraulic and stomatal functions, thus leading to lower ET and higher mortality risk than the estimates here. Future work is required to quantify the influence of trait plasticity on the responses of ET and mortality risk to water stresses.

4.3. Ecosystem water use under dynamic water stresses and coupling with vulnerability

As suggested by Feng et al. (2017), the responses of ecosystem vulnerability and water flux are not always coupled under stress. Our analysis here specifies that the coupling between water flux and vulnerability depends on both the stress regime and the source of risk. At both sites, under high VPD conditions, variations of ET and SCR in response to GWT are coupled, except when GWT becomes extremely low. Likewise, the responses of HFR and ET to GWT are coupled under moderate to high VPD, but decoupled under minimum VPD (Fig. S5). Therefore, predicting ecosystem water flux and vulnerability requires estimation of site-specific stress regime and improved understanding of mortality mechanism.

The systematic scenario analysis predicts the combined effects of co-occurrence of soil and atmospheric water stresses on ET. We identified the stress domain where ET is promoted (through diffusion gradient) and limited (through stomata) by VPD, respectively. ET first increases and then decreases as VPD exceeds a threshold. This threshold, notably, reduces as soil water stress intensifies. These findings highlight that constraining the uncertainty of subsurface hydrological conditions, which is arguably more uncertain, is as important as quantifying VPD change to predict ecosystem ET under future climate. Besides, our analysis also highlights that, ecosystem water flux and mortality risk, although both resulting from hydraulic dynamics, are not always coupled, depending on specific stress regime and mortality mechanism. Our analysis systematically assessed multiple aspects of eco-physiological functions in response to joint soil and atmospheric water stresses, which will provide insights for water resource and risk management of Dryland riparian ecosystems.

5. Conclusions

This study used a plant hydraulic model to estimate the hydraulic sensitivities, tree mortality risk and evapotranspiration of two desert riparian ecosystems. We derived the hydraulic traits at an ecosystem-scale using a model-data fusion approach, which enables the model to capture observed plant hydraulic dynamics as reflected by leaf water potential, sap-flow and evapotranspiration. Starting from the observed soil and atmospheric water stresses, we generated a wide range of stress scenarios to evaluate the individual and compound impacts of water stresses. The results highlight low plant hydraulic sensitivities under high water stresses, and the strong coupled impact of co-occurrence of soil and atmospheric water stresses on restricting ecosystem water flux and intensifying mortality risk. Ecosystem water flux and mortality risk, although both resulting from hydraulic dynamics, are not always coupled, depending on specific stress regime and mortality mechanism. Our analysis assessed multiple aspects of eco-physiological functions under dynamic soil and atmospheric water stresses in desert riparian ecosystems. The findings will contribute to a better prediction of Dryland ecosystem functions and facilitate water resource management under future climate.

Declaration of Competing Interest

The authors declare that they have no known competing financial interests or personal relationships that could have appeared to influence the work reported in this paper.

Acknowledgements

This research was financially supported by the National Natural Science Foundation of China (Grant Nos. 41991231, 42101023, and 42041004). Yan Bai acknowledges support from all the scientists and students who participated in the HiWATER field campaigns. This research used the Savio computational cluster resource provided by the Berkeley Research Computing program at the University of California, Berkeley (supported by the UC Berkeley Chancellor, Vice Chancellor for Research, and Chief Information Officer).

Supplementary materials

Supplementary material associated with this article can be found, in the online version, at doi:10.1016/j.agrformet.2021.108701.

References

Ahlström, A., Raupach, M.R., Schurgers, G., Smith, B., Arneth, A., Jung, M., Reichstein, M., Canadell, J.G., Friedlingstein, P., Jain, A.K., 2015. The dominant role of semi-arid ecosystems in the trend and variability of the land CO_2 sink. Science 348, 895–899.

Allen, C.D., Macalady, A.K., Chenchouni, H., Bachelet, D., McDowell, N., Vennetier, M., Kitzberger, T., Rigling, A., Breshears, D.D., Hogg, E.H, Gonzalez, P., Fensham, R., Zhang, Z., Castro, J., Demidova, N., Lim, J.H., Allard, G., Running, S.W., Semerci, A., Cobb, N., 2010. A global overview of drought and heat-induced tree mortality reveals emerging climate change risks for forests. For. Ecol. Manag. 259, 660–684.

Anderegg, W.R.L., Venturas, M.D., 2020. Plant hydraulics play a critical role in Earth system fluxes. New Phytol. 6, 1535–1538.

Anderegg, W.R.L., Wolf, A., Arango-Velez, A., Choat, B., Chmura, D.J., Jansen, S., Kolb, T., Li, S., Meinzer, F., Pita, P., Resco de Dios, V., Sperry, J.S., Wolfe, B.T., Pacala, S., 2017. Plant water potential improves prediction of empirical stomatal models. PLoS ONE 12, 1–17.

Ayup, M., Chen, Y.N., Nyongesah, M.J., Zhang, Y.M., Rajput, V.D., Zhu, .C.G., 2015. Xylem anatomy and hydraulic traits of two co-occurring riparian desert plants. IAWA J. 36, 69–83.

Bai, Y., Li, X., Liu, S., Wang, P., 2017. Modeling diurnal and seasonal hysteresis phenomena of canopy conductance in an oasis forest ecosystem. Agric. For. Meteorol. 246, 98–110.

Bai, Y., Liu, Y., Kueppers, L.M., Feng, X., Powell, T.L., Li, E., Zhang, C., Yang, X., Li, X., 2021. Distinct hydraulic and stomatal regulations masked by convergent anisohydric behaviors in two desert riparian ecosystems. Under review.
Biederman, J.A., Scott, R.L., Bell, T.W., Bowling, D.R., Dore, S., Garatuza-Payan, J., Kolb, T.E., Krishnan, P., Krofcheck, D.J., Litvak, M.E., Maurer, G.E., Meyers, T.P., Oechel, W.C., Papuga, S.A., Ponce-Campos, G.E., Rodriguez, J.C., Smith, W.K., Vargas, R., Watts, C.J., Yepez, E.A., Goulden, M.L., 2017. CO_2 exchange and evapotranspiration across Dryland ecosystems of southwestern North America. Glob. Chang. Biol. 23, 4204–4221.
Bjorkman, A.D., Myers-Smith, I.H., Elmendorf, S.C., et al., 2018. Plant functional trait change across a warming tundra biome. Nature 562, 57–62.
Bonan, G.B., 1996. Land surface model (LSM version 1.0) for ecological, hydrological, and atmospheric studies: technical description and users guide. Technical note. National Center for Atmospheric Research, Boulder, CO (United States).
Bonan, G.B., Williams, M., Fisher, R.A., Oleson, K.W., 2014. Modeling stomatal conductance in the earth system: linking leaf water-use efficiency and water transport along the soil-plant-atmosphere continuum. Geosci. Model Dev. 7, 2193–2222.
Breshears, D.D., Cobb, N.S., Rich, P.M., Price, K.P., Allen, C.D., Balice, R.G., Romme, W. H., Kastens, J.H., Floyd, M.L., Belnap, J., Anderson, J.J., Myers, O.B., Meyer, C.W., 2005. Regional vegetation die-off in response to global-change-type drought. Proc. Natl. Acad. Sci. USA. 102, 15144–15148.
Brodribb, T.J., Holbrook, N.M., Edwards, E.J., Gutiérrez, M.V., 2003. Relations between stomatal closure, leaf turgor and xylem vulnerability in eight tropical dry forest trees. Plant Cell Environ. 26, 443–450.
Brodribb, T.J., Powers, J., Cochard, H., Choat, B., 2020. Hanging by a thread? Forests and drought. Science 368, 261–266.
Brooks, S.P., Gelman, A., 1998. General methods for monitoring convergence of iterative simulations. J. Comput. Graph. Stat. 7, 434–455.
Brouillette, L.C., Mason, C.M., Shirk, R.Y., Donovan, L.A., 2014. Adaptive differentiation of traits related to resource use in a desert annual along a resource gradient. New Phytol. 201, 1316–1327.
Campbell, G.S., Norman, J., 2012. An Introduction to Environmental Biophysics. Springer Science & Business Media.
Choat, B., Brodribb, T.J., Brodersen, C.R., Duursma, R.A., López, R., Medlyn, B.E., 2018. Triggers of tree mortality under drought. Nature 558, 531–539.
Christoffersen, B.O., Gloor, M., Fauset, S., Fyllas, N.M., Galbraith, D.R., Baker, T.R., Kruijt, B., Rowland, L., Fisher, R.A., Binks, O.J., Sevanto, S., Xu, C., Jansen, S., Choat, B., Mencuccini, M., McDowell, N.G., Meir, P., 2016. Linking hydraulic traits to tropical forest function in a size-structured and trait-driven model (TFS v.1-Hydro). Geosci. Model Dev. 9, 4227–4255.
Clapp, R.B., Hornberger, G.M., 1978. Empirical equations for some soil hydraulic properties. Water Resour. Res. 14, 601–604.
Farquhar, G.D., von Caemmerer, S., Berry, J.A., 1980. A biochemical model of photosynthetic CO_2 assimilation in leaves of C3 species. Planta 149, 78–90.
Feng, X., Ackerly, D.D., Dawson, T.E., Manzoni, S., McLaughlin, B., Skelton, R.P., Vico, G., Weitz, A.P., Thompson, S.E., 2019. Beyond isohydricity: the role of environmental variability in determining plant drought responses. Plant Cell Environ. 42, 1104–1111.
Feng, X., Dawson, T.E., Ackerly, D.D., Santiago, L.S., Thompson, S.E., 2017. Reconciling seasonal hydraulic risk and plant water use through probabilistic soil–plant dynamics. Glob. Chang. Biol. 23, 3758–3769.
Ficklin, D.L., Novick, K.A., 2017. Historic and projected changes in vapor pressure deficit suggest a continental-scale drying of the United States atmosphere. J. Geophys. Res. Atmos. 122, 2061–2079.
Guo, J.S., Hultine, K.R., Koch, G.W., Kropp, H., Ogle, K., 2020. Temporal shifts in iso/anisohydry revealed from daily observations of plant water potential in a dominant desert shrub. New Phytol. 225, 713–726.
Hochberg, U., Rockwell, F.E., Holbrook, N.M., Cochard, H., 2018. Iso/Anisohydry: a plant–environment interaction rather than a simple hydraulic trait. Trends Plant Sci. 23, 112–120.
Hu, Z., Yu, G., Zhou, Y., Sun, X., Li, Y., Shi, P., Wang, Y., Song, X., Zheng, Z., Zhang, L., Li, S., 2009. Partitioning of evapotranspiration and its controls in four grassland ecosystems: application of a two-source model. Agric. For. Meteorol. 149, 1410–1420.
Huang, C.W., Domec, J.C., Ward, E.J., Duman, T., Manoli, G., Parolari, A.J., Katul, G.G., 2017. The effect of plant water storage on water fluxes within the coupled soil–plant system. New Phytologist 213, 1093–1106.
IPCC, 2013: Climate Change 2013: The Physical Science Basis (eds Stocker, T. F. et al.) (Cambridge Univ. Press, 2013).
Jackson, R.B., Mooney, H.A., Schulze, E.D., 1997. A global budget for fine root biomass, surface area, and nutrient contents. Proc. Natl. Acad. Sci. USA. 94, 7362–7366.
Ji, C., Schmidler, S.C., 2013. Adaptive Markov chain Monte Carlo for Bayesian variable selection. J. Comput. Graph. Stat. 22, 708–728.
Katul, G., Leuning, R., Oren, R., 2003. Relationship between plant hydraulic and biochemical properties derived from a steady-state coupled water and carbon transport model. Plant Cell Environ. 26, 339–350.
Katul, G.G., Palmroth, S., Oren, R., 2009. Leaf stomatal responses to vapour pressure deficit under current and CO_2-enriched atmosphere explained by the economics of gas exchange. Plant Cell Environ. 32, 968–979.
Klein, T., Niu, S., 2014. The variability of stomatal sensitivity to leaf water potential across tree species indicates a continuum between isohydric and anisohydric behaviours. Funct. Ecol. 28, 1313–1320.
Klein, T., Zeppel, M.J.B., Anderegg, W.R.L., Bloemen, J., De Kauwe, M.G., Hudson, P., Ruehr, N.K., Powell, T.L., von Arx, G., Nardini, A., 2018. Xylem embolism refilling and resilience against drought-induced mortality in woody plants: processes and trade-offs. Ecol. Res. 33, 839–855.
Keenan, T.F., Niinemets, Ü., 2016. Global leaf trait estimates biased due to plasticity in the shade. Nat. Plants 3, 1–6.
Kulmatiski, A., Yu, K., Mackay, D.S., Holdrege, M.C., Staver, A.C., Parolari, A.J., Liu, Y., Majumder, S., Trugman, A.T., 2020. Forecasting semi-arid biome shifts in the Anthropocene. New Phytol. 226, 351–361.
Lal, R., 2004. Carbon sequestration in Dryland ecosystems. Environ. Manag. 33, 528–544.
Li, E., Tong, Y., Huang, Y., Li, X., Wang, P., Chen, H., Yang, C., 2019a. Responses of two desert riparian species to fluctuating groundwater depths in hyperarid areas of Northwest China. Ecohydrology 12, 1–12.
Li, X., Blackman, C.J., Peters, J.M.R., Choat, B., Rymer, P.D., Medlyn, B.E., Tissue, D.T., 2019b. More than iso/anisohydry: hydroscapes integrate plant water use and drought tolerance traits in 10 eucalypt species from contrasting climates. Funct. Ecol. 33, 1035–1049.
Li, X., Liu, S., Xiao, Q., Ma, M., Jin, R., Che, T., Wang, W., Hu, X., Xu, Z., Wen, J., Wang, L., 2017. A multiscale dataset for understanding complex eco-hydrological processes in a heterogeneous oasis system. Sci. Data 4, 1–11.
Liu, Y., Holtzman, N.M., Konings, A.G., 2020a. Global ecosystem-scale plant hydraulic traits retrieved using model-data fusion. Hydrol. Earth Syst. Sci. 1–30.
Liu, Y., Kumar, M., Katul, G.G., Feng, X., Konings, A.G., 2020b. Plant hydraulics accentuates the effect of atmospheric moisture stress on transpiration. Nat. Clim. Chang. 10, 691–695.
Liu, Y., Parolari, A.J., Kumar, M., Huang, C.W., Katul, G.G., Porporato, A., 2017. Increasing atmospheric humidity and CO_2 concentration alleviate forest mortality risk. Proc. Natl. Acad. Sci. USA. 114, 9918–9923.
López, R., Cano, F.J., Choat, B., Cochard, H., Gil, L., 2016. Plasticity in vulnerability to cavitation of *Pinus canariensis* occurs only at the driest end of an aridity gradient. Front. Plant. Sci. 7, 1–10.
Manzoni, S., Katul, G., Porporato, A., 2014. A dynamical system perspective on plant hydraulic failure. Water Resour. Res. 50, 5170–5183.
Manzoni, S., Vico, G., Katul, G., Fay, P.A., Polley, W., Palmroth, S., Porporato, A., 2011. Optimizing stomatal conductance for maximum carbon gain under water stress: a meta-analysis across plant functional types and climates. Funct. Ecol. 25, 456–467.
Martínez-Vilalta, J., Poyatos, R., Aguadé, D., Retana, J., Mencuccini, M., 2014. A new look at water transport regulation in plants. New Phytol. 204, 105–115.
Matheny, A.M., Fiorella, R.P., Bohrer, G., Poulsen, C.J., Morin, T.H., Wunderlich, A., Vogel, C.S., Curtis, P.S., 2017. Contrasting strategies of hydraulic control in two codominant temperate tree species. Ecohydrology 10, 1–16.
McDowell, N.G., Allen, C.D., 2015. Darcy's law predicts widespread forest mortality under climate warming. Nat. Clim. Chang. 5, 669–672.
Mcdowell, N.G., Fisher, R.A., Xu, C., et al., 2013. Evaluating theories of drought-induced vegetation mortality using a multimodel-experiment framework. New Phytol. 200, 304–321.
McDowell, N.G., Brodribb, T.J., Nardini, A., 2019. Hydraulics in the 21st century. New Phytol. 224, 537–542.
McLaughlin, B.C., Ackerly, D.D., Klos, P.Z., Natali, J., Dawson, T.E., Thompson, S.E., 2017. Hydrologic refugia, plants, and climate change. Glob. Chang. Biol. 23, 2941–2961.
Miller, G.R., Chen, X., Rubin, Y., Ma, S., Baldocchi, D.D., 2010. Groundwater uptake by woody vegetation in a semiarid oak savanna. Water Resour. Res. 46, 1–14.
Mirfenderesgi, G., Bohrer, G., Matheny, A.M., Fatichi, S., de Moraes Frasson, R.P., Schäfer, K.V.R., 2016. Tree level hydrodynamic approach for resolving aboveground water storage and stomatal conductance and modeling the effects of tree hydraulic strategy. J. Geophys. Res. Biogeosci. 121, 1792–1813.
Mrad, A., Domec, J.C., Huang, C.W., Lens, F., Katul, G., 2018. A network model links wood anatomy to xylem tissue hydraulic behaviour and vulnerability to cavitation. Plant Cell Environ. 41, 2718–2730.
Niu, G., Yang, Z., Mitchell, K.E., Chen, F., Ek, M.B., Barlage, M., Kumar, A., Manning, K., Niyogi, D., Rosero, E., 2011. The community Noah land surface model with multiparameterization options (Noah-MP): 1. Model description and evaluation with local-scale measurements. J. Geophys. Res. Atmos. 116.
North, G.B., Peterson, C.A., 2005. Water flow in roots: structural and regulatory features. Vascular Transport in Plants. Elsevier, pp. 131–156.
Oleson, K.W., Lawrence, D.M., Gordon, B., Flanner, M.G., Kluzek, E., Peter, J., Levis, S., Swenson, S.C., Thornton, E., Feddema, J., 2010. Technical description of version 4.0 of the community land model (CLM).
Poulter, B., Frank, D., Ciais, P., Myneni, R.B., Andela, N., Bi, J., Broquet, G., Canadell, J. G., Chevallier, F., Liu, Y.Y., Running, S.W., Sitch, S., Van Der Werf, G.R., 2014. Contribution of semi-arid ecosystems to interannual variability of the global carbon cycle. Nature 509, 600–603.
Reed, S.C., Coe, K.K., Sparks, J.P., Housman, D.C., Zelikova, T.J., Belnap, J., 2012. Changes to Dryland rainfall result in rapid moss mortality and altered soil fertility. Nat. Clim. Chang. 2, 752–755.
Rieger, M., Litvin, P., 1999. Root system hydraulic conductivity in species with contrasting root anatomy. J. Exp. Bot. 50, 201–209.
Schlaepfer, D.R., Bradford, J.B., Lauenroth, W.K., Munson, S.M., Tietjen, B., Hall, S.A., Wilson, S.D., Duniway, M.C., Jia, G., Pyke, D.A., Lkhagva, A., Jamiyansharav, K., 2017. Climate change reduces extent of temperate Drylands and intensifies drought in deep soils. Nat. Commun. 8, 1–9.
Sellers, P.J., Randall, D.A., Collatz, G.J., Berry, J.A., Field, C.B., Dazlich, D.A., Zhang, C., Collelo, G.D., Bounoua, L., 1996. A revised land surface parameterization (SiB2) for atmospheric GCMs. Part I: model formulation. J. Clim. 9, 676–705.
Shuttleworth, W.J., Wallace, J.S., 1985. Evaporation from sparse crops-an energy combination theory. Q. J. R. Meteorol. Soc. 111, 839–855.

Skelton, R.P., West, A.G., Dawson, T.E., 2015. Predicting plant vulnerability to drought in biodiverse regions using functional traits. Proc. Natl. Acad. Sci. USA. 112, 5744–5749.
Song, L., Bian, Z., Kustas, W.P., Liu, S., Xiao, Q., Nieto, H., Xu, Z., Yang, Y., Xu, T., Han, X., 2020. Estimation of surface heat fluxes using multi-angular observations of radiative surface temperature. Remote Sens. Environ. 239, 111674.
Song, L., Liu, S., Kustas, W.P., Nieto, H., Sun, L., Xu, Z., Skaggs, T.H., Yang, Y., Ma, M., Xu, T., Tang, X., Li, Q., 2018. Monitoring and validating spatially and temporally continuous daily evaporation and transpiration at river basin scale. Remote Sens. Environ. 219, 72–88.
Sperry, J.S., Hacke, U.G., 2002. Desert shrub water relations with respect to soil characteristics and plant functional type. Funct. Ecol. 16, 367–378.
Sperry, J.S., Love, D.M., 2015. What plant hydraulics can tell us about responses to climate-change droughts. New Phytol. 207, 14–27.
Sperry, J.S., Venturas, M.D., Anderegg, W.R.L., Mencuccini, M., Mackay, D.S., Wang, Y., Love, D.M., 2017. Predicting stomatal responses to the environment from the optimization of photosynthetic gain and hydraulic cost. Plant Cell Environ. 40, 816–830.
Stromberg, J.C., McCluney, K.E., Dixon, M.D., Meixner, T., 2013. Dryland riparian ecosystems in the American Southwest: sensitivity and resilience to climatic extremes. Ecosystems 16, 411–415.
Tramontini, S., Döring, J., Vitali, M., Ferrandino, A., Stoll, M., Lovisolo, C., 2014. Soil water-holding capacity mediates hydraulic and hormonal signals of near-isohydric and near-anisohydric Vitis cultivars in potted grapevines. Funct. Plant Biol. 41, 1119–1128.
Trugman, A.T., Medvigy, D., Mankin, J.S., Anderegg, W.R.L., 2018. Soil moisture stress as a major driver of carbon cycle uncertainty. Geophys. Res. Lett. 45, 6495–6503.
Wu, H., Zhao, G., Li, X.Y., Wang, Y., He, B., Jiang, Z., Zhang, S., Sun, W., 2019. Identifying water sources used by alpine riparian plants in a restoration zone on the Qinghai-Tibet Plateau: evidence from stable isotopes. Sci. Total Environ. 697, 134092.
Wu, G., Guan, K., Li, Y., Novick, K.A., Feng, X., McDowell, N.G., Konings, A.G., Thompson, S.E., Kimball, J.S., De Kauwe, M.G., Ainsworth, E.A., Jiang, C., 2021. Interannual variability of ecosystem iso/anisohydry is regulated by environmental dryness. New Phytol. 229, 2562–2575.
Yu, T., Qi, F., Si, J., Zhang, X., Zhao, C., 2017. Tamarix ramosissima stand evapotranspiration and its association with hydroclimatic factors in an arid region in northwest China. J. Arid Environ. 138, 18–26.
Yuan, W., Zheng, Y., Piao, S., Ciais, P., Lombardozzi, D., Wang, Y., Ryu, Y., Chen, G., Dong, W., Hu, Z., 2019. Increased atmospheric vapor pressure deficit reduces global vegetation growth. Sci. Adv. 5, eaax1396.
Zhang, C., Li, X., Wu, H., Wang, P., Wang, Y., Wu, X., Li, W., Huang, Y., 2017. Differences in water-use strategies along an aridity gradient between two coexisting desert shrubs (Reaumuria soongorica and Nitraria sphaerocarpa): isotopic approaches with physiological evidence. Plant Soil 419, 169–187.
Zhou, S., Williams, A.P., Lintner, B.R., Berg, A.M., Zhang, Y., Keenan, T.F., Cook, B.I., Hagemann, S., Seneviratne, S.I., Gentine, P., 2021. Soil moisture–atmosphere feedbacks mitigate declining water availability in Drylands. Nat. Clim. Chang. 11, 38–44.
Zhu, J., Yu, J., Wang, P., Zhang, Y., Yu, Q., 2012. Interpreting the groundwater attributes influencing the distribution patterns of groundwater-dependent vegetation in northwestern China. Ecohydrology 5, 628–636.